SUMMER STUDENT INTERNSHIP

FINAL REPORT

LArCADe: ATTEMPT TO OBTAIN A SINGLE PHASE TPC WITH LIQUID ARGON

Supervisors: Dr Angela Fava and Dr David Caratelli

Student: Sara Leardini

31 July - 28 September 2018

Contents

Abstract **5**

1 Literature review **7**
1.1 Time Projection Chambers 7
1.1.1 Determination of nuclear recoil 8
1.1.2 Single-phase and dual-phase TPCs 10
1.1.3 Attempts to build a single-phase TPC with stable amplification of electrons 11

2 LArCADe measurements and simulations **15**
2.1 Experimental apparatus 15
2.2 Run 1 17
2.3 Run 2 21
2.3.1 Multiplication factor in LAr 25
2.4 Simulations with COMSOL 26
2.4.1 Setup of the simulation 27
2.4.2 Analysis of the simulated data 30
2.5 Run 3 31
2.6 Setup of Raspberry Pi camera 33

3 Conclusions **35**

Bibliography **37**

Abstract

Time Projection Chambers (TPCs) are detectors widely used in particle physics experiments; they often use liquid noble elements as scintillating material due to their high scintillation and ionization yield. In principle, when a particle interacts with the scintillating material, it produces two signals, the former due to a mixture of excited and ionized atoms, and the latter due to ionized atoms only; in practice, nevertheless, to detect the second signal, some amplification is needed, which is very difficult to obtain in a stable form in liquid. For this reason, to date for low energy threshold experiments dual-phase TPCs are employed, which contain also a small volume of gaseous noble element to amplify the ionization signal; nevertheless, they require technical efforts to control the interface between the gas and the liquid, and yield worse performances as far as spatial resolution is concerned. A way to overcome these problems would be to obtain stable electron amplification in only liquid TPCs (single-phase TPCs), which nowadays are limited to the noise levels of the electronics instead. This would allow to reach energy thresholds of the order of tens of keV, making it possible to employ them for paramount experiments in particle physics, such as WIMP direct detection experiments, and neutrino coherent scattering experiments. The project presented is placed in this framework: LArCADe is indeed an R&D project, which aims to obtain stable electron amplification in liquid Argon immersing small tips (with radius $\sim$ 15 μm) in an electric field, in order to locally increase the electric field itself, exploiting the convergence of field lines onto the tips. The work described in the report was performed in August and September 2018, during an internship offered by the "Italian program at the Fermi National Accelerator Laboratory and at other US Laboratories". Although no amplification in liquid Argon was observed during the internship, the work was useful to calibrate future measurements, and to deepen the understanding of the experimental setup, also thanks to some simulations that were performed.
The contents of the report are organized as follows: in Chapter 1 some literature will be revised, explaining in more detail what a TPC is, the difference between a dual-phase and a single-phase TPC, the effect of the interaction of a particle with the noble element atoms and previous attempts to build a single-phase TPC with stable amplification; in Chapter 2 the work performed

during the internship is presented: the improvement of a previously developed data analysis method, two data takings in liquid and gaseous Argon with tips, a simulation of a simplified version of the experimental apparatus with the software COMSOL, and the setup of a Raspberry Pi camera to monitor the tips in a future run.

Chapter 1

Literature review

In this Chapter, the operation of a Time Projection Chamber (TPC) will be described, reporting also some works about the determination of electron production by nuclear recoil; the differences between a single-phase and a dual-phase TPC will then be explained, and finally some attempts to build a single-phase TPC with stable amplification of electrons will be illustrated.

1.1 Time Projection Chambers

A Time Projection Chamber (TPC) is a detector that uses a volume filled with a sensitive material to detect the passage of a particle. In this work the focus will be on TPCs which use noble elements, typically Argon or Xenon, as the sensitive material; they let, in principle, collect two kind of signals: when the particle interacts with the medium, in fact, two phenomena take place, excitation of some atoms, and ionization of others. The first phenomenon produces scintillation light, which can be collected through photomultipliers, generating a first signal called "S1"; the second phenomenon, together with the application of an electric field, gives rise to a drift of electrons, that can be detected in two ways: either collecting them directly or, exploiting electroluminescence, using photomultipliers as for S1; this second signal is called "S2". During the drift the number of photons/electrons can eventually increase through a cascade effect; on the other hand, phenomena such as diffusion of electrons, Rayleigh scattering, and photon absorption decrease the number of detected electrons/photons (Chepel & Araújo, 2013); besides, one fact to keep in mind is that some of the ionization electrons recombine producing primary scintillation light, causing the detection of an increased S1 and a depleted S2.
The time difference between S1 and S2 provides the depth coordinate of the particle interaction point with the medium, while the other two spatial coordinates can be given by the photomultipliers that are hit, or by the wires that collect the electrons, if there exist at least two layers of wires, with different

orientations. If the number of photons/electrons detected in S1 and S2 is somehow proportional to the number of initially produced photons/electrons it is also possible to reconstruct the energy of the particle.

1.1.1 Determination of nuclear recoil

When a particle interacts with a noble element's atoms in the TPC, it could collide either with an electron (producing an *electron recoil*, ER) or with a nucleus (producing a *nuclear recoil*, NR): sufficiently energetic ERs transfer energy uniquely to excite and ionize atoms (at too low energies they collide with atoms and heat the medium); in NR, on the other hand, the largest fraction of energy is transferred to nuclei, at the expense of the number of ionized/excited electrons. In experiments investigating WIMP Dark Matter or Neutrino Coherent Scattering, all events yielding ER are sources of background; moreover, some events with NR are also background, since NR can be caused also by α particles coming from natural radioactivity and atmospheric-muons-induced neutrons.
If both S1 and S2 are available, it is quite easy to discriminate NRs from ERs; in fact, the ratio between the number of excited electrons N_e and ionized electrons N_i is ~ 0.2 for ER, while for NR it becomes ~ 1 (Chepel & Araújo, 2013); taking into account the factors that may modify the ratio during the drift, described in previous Section, measuring the magnitude of S1 and S2 allows to determine whether the signal was due to a ER or a NR. This technique is widely used with dual-phase TPC experiments.
Another method to tell an ER from a NR is called *Pulse Shape Discrimination* (PSD), which allows to distinguish the two different recoils exploiting S1 only. PSD relies on the fact that, when a particle interacts with a noble element atom (both in case of excitation and ionization), an excited molecule made of two atoms form (called *excimer*); the excimer will eventually dissociate again into two atoms, emitting a photon. The excimer, nevertheless, can exist in two different states, which are spectroscopically identical but have different decay times (Chepel & Araújo, 2013): the long lived triplet state and the short lived singlet state (the decay times obviously vary depending on the noble element considered). ERs and NRs contain a different ratio between the two states, which is reflected in the scintillation signal collected over time. This technique is very useful for single phase detectors collecting only S1, such as DEAP-3600 (DEAP-3600 Collaboration, 2018).
Another fundamental issue is the response of liquid Argon to ER and NR; for example, to develop the TPC describer in this work it is important to know the number of electrons produced for each NR, in order to calculate the multiplication required to detect S2. As a starting point, the work by the ARIS Collaboration (2018) was considered; they built a small single-phase detector with liquid Argon, to probe the response of Argon to ERs and NRs. The device was exposed to two different recoil sources, one producing a γ

photon beam and the other providing a neutron beam, both of fixed energy; eight scintillators, placed at known angles with respect to the beams, collected the particles after they collided with Argon atoms, to measure the recoil energy. They collected data with null electric field, and then tried to determine the scintillation efficiency for NRs, L_{eff} trying to fit the data with different expressions:

1) The Lindhard expression:

$$L_{eff}^{L} = \frac{k \cdot g(\epsilon)}{1 + k \cdot g(\epsilon)} \tag{1.1}$$

where $k = 0.133\, Z^{2/3}\, A^{-1/2}$, $\epsilon = 11.5\, E_{NR} Z^{-7/3}$ and $g(\epsilon) = 3\epsilon^{0.15} + 0.7\epsilon^{0.6} + \epsilon$. E_{NR} is in keV, while Z and A are respectively the atomic number and the mass number.

2) The Mei expression:

$$L_{eff}^{M} = L_{eff}^{L} \cdot \frac{1}{1 + k_B \cdot \frac{dE}{dx}} \tag{1.2}$$

where $k_B = 7.4 \cdot 10^{-4}$ MeV^{-1} g cm^{-2}.

3) A modified Mei expression:

$$L_{eff}^{MM} = L_{eff}^{L} \cdot \frac{1}{1 + k_B \cdot \frac{dE}{dx} + k_B^{M} \cdot (\frac{dE}{dx})^2} \tag{1.3}$$

where $k_B = (5.2 \pm 0.6) \cdot 10^{-4}$ MeV^{-1} g cm^{-2} and $k_B^{M} = (-2.0 \pm 0.7) \cdot 10^{-7}$ MeV^{-2} g^2 cm^{-4}.

While the Lindhard and the Mei expressions did not fit accurately enough the data, the modified Mei expression turned out to be compatible (Figure 1.1, left). A further data set was taken afterwards, setting an electric field at 50, 100, 200, and 500 V/cm, in order to prevent the recombination of ionization electrons; this allowed to estimate the number of ionization electrons with a tuned Thomas-Imel model:

$$N_e = L_{eff}^{MM} \cdot \frac{E_{dep}}{W} \cdot \frac{1 - R(E_{ee}, F)}{1 + \alpha} \tag{1.4}$$

where $W = 19.5$ eV is the effective work function, α is the ratio between excited and ionized electrons and is assumed equal to 1 for NR, and R is the recombination probability. The possibility to fit the data with this expression (Figure 1.1, right) seems to indicate that, apart from L_{eff}^{MM} there are no other quenching factors acting on S2.

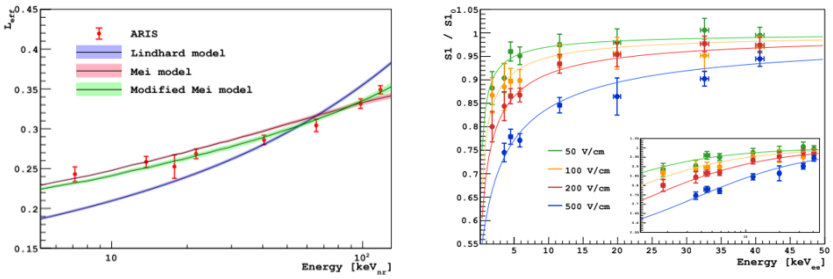

Figure 1.1: Left: fit of L_{eff} data acquired by ARIS Collaboration with null electric field with the Lindhard, Mei and modified Mei expressions. Right: S1 data relative to different electric fields fitted with a Thomas-Imel model; the fact that the only quenching factor seems to be L_{eff}^{MM} allows to use the model to predict the number of ionization electrons. Both plots are from the ARIS Collaboration (2018).

1.1.2 Single-phase and dual-phase TPCs

There are two different types of noble-gas TPCs that are currently used in experiments:

- the *dual-phase* TPC, which makes use of a volume of liquid noble gas beneath a layer of the same material, but in the gas phase. The S1 signal is typically reflected at the interface liquid-gas and is detected almost entirely by photomultipliers put in the opposite side; the electrons, instead, can cross the interface thanks to the application of two different electric fields in the liquid and in the gas part. Once in the gas, they cause a proportional scintillation, detectable by photomultipliers above the area. An example of this kind of dual-phase TPC is shown in Figure 1.2, illustrating the two signals S1 and S2; nowadays this technology is widely used for experiments looking for Dark Matter, such as XENON and LUX.
  Another way to collect the S2 signal, as mentioned above, is to detect the electrons directly, for example with wires or strips. In the gaseous part of the dual-phase TPC electrons ionize other atoms and produce an avalanche with the help of Electron Multipliers (Murphy, 2016).

- the *single-phase* TPC, which uses only the liquid phase. Some experiments that make use of this technology are MicroBooNE and Icarus, which study neutrino oscillations (see Figure 1.3 for a scheme of MicroBooNE).

Despite being a widely employed technology, and being so useful for low-energy threshold experiments such as those looking for Dark Matter particles and neutrino coherent scattering, dual-phase TPCs pose some disadvantages: for example, constraints when designing the experiment since it is necessary

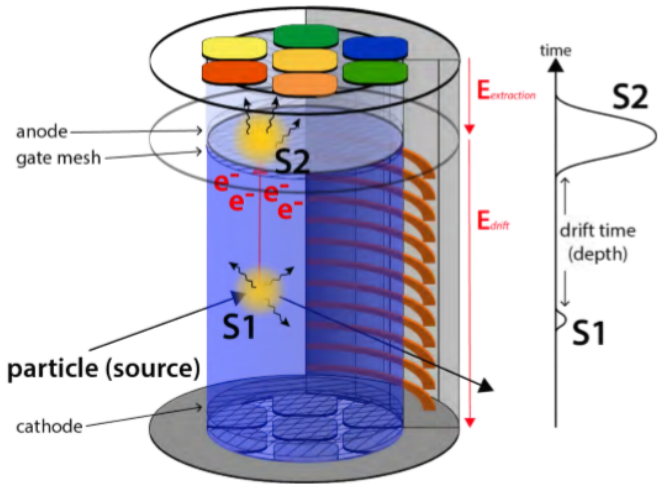

Figure 1.2: Scheme of a dual-phase TPC, showing the passage of a particle and the production of S1 and S2 signals; in this case both signals are collected through photomultipliers (Althüser, 2015).

to control the interface between liquid and gas, with a quiet surface and constant and uniform temperature and pressure (Chepel & Araújo, 2013); the total reflection of photons at the interface lowers the light collection efficiency for the S1 signal (Aprile et al., 2014); liquid only would provide better spatial resolution, one reason being the denser medium and hence the smaller diffusion allowed (Kim et al., 2002). Using a single-phase TPC would overcome these problems; on the other hand, so far attempts to build a single-phase TPC with stable electron amplification, or a good signal from electroluminescence, have been unsuccessful (Chepel & Araújo, 2013). This limits the use of single-phase TPC to higher energy thresholds experiments, since the detection of the unamplified S2 signal is constrained by the signal-to-noise ratio of electronic devices.

1.1.3 Attempts to build a single-phase TPC with stable amplification of electrons

As mentioned before, building a single-phase TPC with stable amplification of electrons would expand the physics reach of this device, allowing to employ it in place of dual-phase TPCs, avoiding the listed drawbacks. Some attempts to reach this goal were made throughout the years, and here follows a description of some experiments performed with this aim, although they will be only some examples and not an exhaustive list.

Policarpo et al. (1995) tried to obtain stable electron amplification in liquid Xenon: a microstrip chamber was used, filled with the liquid, and containing

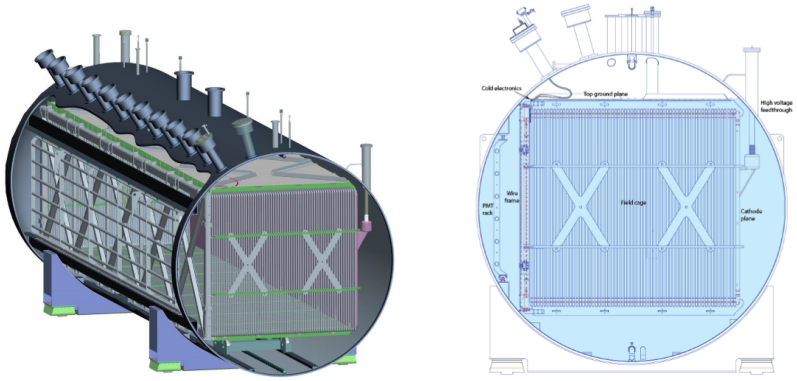

Figure 1.3: Scheme of MicroBooNE's single-phase TPC: on the left, the TPC is shown as a whole inside a cryostat; the cathode is placed on the right of the TPC with respect to the image, while three layers of wires and photomultipliers are placed on the left; the three distinct wire layers, tilted by 60 degrees one with respect to the other, allow to reconstruct two spatial coordinates. On the right, a section of the TPC is shown; the neutrino beam would exit from the paper, and the ionization electrons would drift towards the left, where the wires and PMTs are placed (MicroBooNE Collaboration, 2012).

a source of α particles (^{241}Am) on a drift electrode; the α particles would interact with xenon atoms, and the S2 signals were collected at the drift electrode, and at the cathode and anode strips at the bottom of the microstrip chamber (Figure 1.4, left). At low anode voltages they observed a single peak at the drift voltage, whose amplitude was proportional to the number of electrons produced which didn't recombine; when they increased the anode voltage, keeping the drift electrode voltage constant, they observed a second peak appearing (Figure 1.4, right). They interpreted this second peak as due to an electron avalanche produced at high electron voltages.

Aprile et al. (2014) succeeded in obtaining both proportional scintillation light and electron multiplication in liquid Xenon. Their experimental setup was a single-phase TPC with a source of α particles (^{210}Po) on the cathode, to excite and ionize Xenon atoms. There were four layers, namely the cathode, a first grid, the anode and an external grid; an electric field was applied between the cathode and the first grid to accelerate the ionization electrons towards the anode, where a stronger electric field was present. The anode was a single wire, whose diameter was 5 μm for a data taking, and 10 μm for another one; two photomultipliers were placed, respectively, behind the cathode and the external grid to collect S1 and S2 photons, while a preamplifier could also measure the number of electrons at the anode. A scheme of the experimental setup is shown in Figure 1.5 (left). Taking data at different anode voltages, they observed the onset of proportional scintillation when the electric field was $E = 412^{+10}_{-133}$ kV/cm, while the threshold to have electron amplification was $E = 725^{+48}_{-139}$ kV/cm (1.5, right). However, the

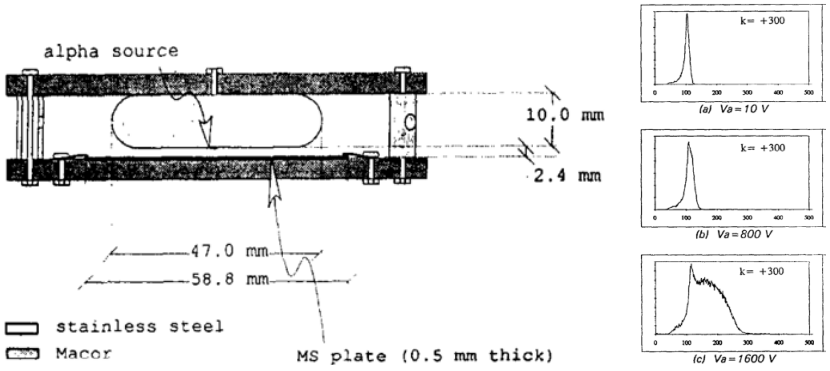

Figure 1.4: Left: scheme of the experimental setup of Policarpo et al. (1995). The anode and the cathode strips are at the bottom, while 1.9 mm away from them there is a drift electrode, with an α source. The cathode is grounded, instead the drift electrode voltage is varied from -450 V to -3000 V; keeping the drift electrode at constant voltage, the anode voltage was varied from 0 V until there was a discharge. Right: example of signals at the drift electrode, keeping the drift electrode voltage constant (-2600 V); when the anode voltage increased, a second peak appeared. Both images are from Policarpo et al. (1995).

electron amplification was basically treated as a disruption to obtain a good resolution for the scintillation signal.

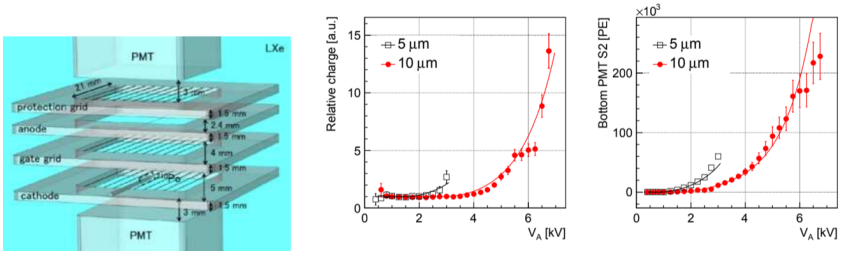

Figure 1.5: Left: scheme of the experimental setup of Aprile et al. (2014). Center: ionization electrons collected at the anode as a function of the anode voltage; when the electric fields reaches values $\sim$ 725 V/cm there is the onset of amplification. Right: proportional scintillation collected at the bottom PMT. Images from Aprile et al. (2014).

Despite these and other results obtained with Xenon, the present work aims at using liquid Argon; in fact, there are some advantages in using this material, since it is much cheaper and quite easy to purify, it allows to discriminate better between electronic and nuclear recoils with the PSD technique, and provides higher nuclear recoil energies because of the lower atomic number (Chepel & Araújo, 2013).
An attempt to obtain stable electron amplification in liquid Argon was carried out by Kim et al. (2002); previous attempts, they point out, produced an unstable amplification, and results depending on the pressure. For their

experiment they installed a cathode between a source of γ rays, ^{241}Am, and a ground plane; on the ground plane a sharp needle (the tip radius was $\sim 0.25\,\mu$m) was attached and acted as the anode. The voltage was changed at the cathode, and varied from 1 kV to 3 kV; finally, a pre-amplifier was connected to the needle, to amplify the signal given by the collected electrons (see a scheme of the setup in Figure 1.6, left).

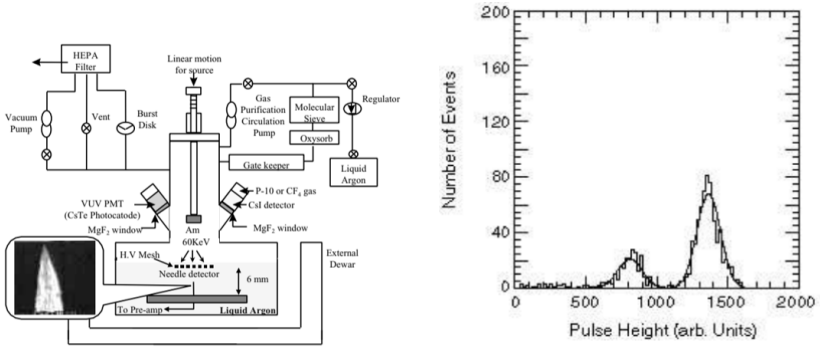

Figure 1.6: Left: scheme of the experimental setup of Kim et al. (2002); in the close up the needle is shown, as seen with an electron microscope. Right: distribution of the amplitudes for the signals obtained in the data-taking, with applied voltage $V = 1750$ V, Xenon concentration 50 ppm and pressure $P = 5$ psi; two distinct peaks are clearly visible, one relative to the smaller, pressure-independent peak and the other to the larger, pressure-dependent peak. Both images are from Kim et al. (2002).

In their experiment, Kim and his colleagues succeeded in producing electron avalanches. Nevertheless, they observed signals which can be either of two types of pulse (Figure 1.6, right): a smaller kind, independent of the pressure,or a larger one, pressure-dependent, the latter interpreted as a sign of a possible formation of bubbles near the needle; the pressure-independent signals, instead, could be indeed relative to amplification in liquid phase. Other problems they faced are, for example, the erratic behavior of the signal in pure liquid Argon, which can appear, disappear, change amplitudes and rate unpredictably; they managed to stabilize the signal by adding a small amount of Xenon. Moreover, the signals are sometimes saturated, which means they don't respect the proportionality with the original ionization electrons.

Chapter 2

LArCADe measurements and simulations

In this Chapter firstly the experimental setup and the results of the measurements taken during Run 1 in April 2018 will be briefly described; then the work which was performed during the internship will be presented: the data acquired during Run 2, both in gaseous and in liquid Argon, then the simulation of the experiment with the software COMSOL, a new run in gaseous Argon and finally the setup of a Raspberry Pi Camera to monitor the experiment in the future.

2.1 Experimental apparatus

The main part of the experimental apparatus is composed of the following parts (see also Figure 2.1):

- Two electrodes, the anode and the cathode;
- Nine optical fibers, whose purpose is to extract electrons from the cathode by the photoelectric effect (Figure 2.2, top); the other end of the fibers is in contact with a UV lamp, that provides the light pulses needed;
- A cathode grid, made of small wires, to screen the electric field near the cathode;
- Two metallic rings, connected together and to the cathode grid through three resistances of 50 MΩ; this makes the electric field almost uniform;
- An anode grid, that, like the cathode grid, has the purpose to screen the electric field;
- Four tips, with a radius of ~ 15 μm, that are soldered to the anode (Figure 2.2, bottom): their presence should increase the electric field

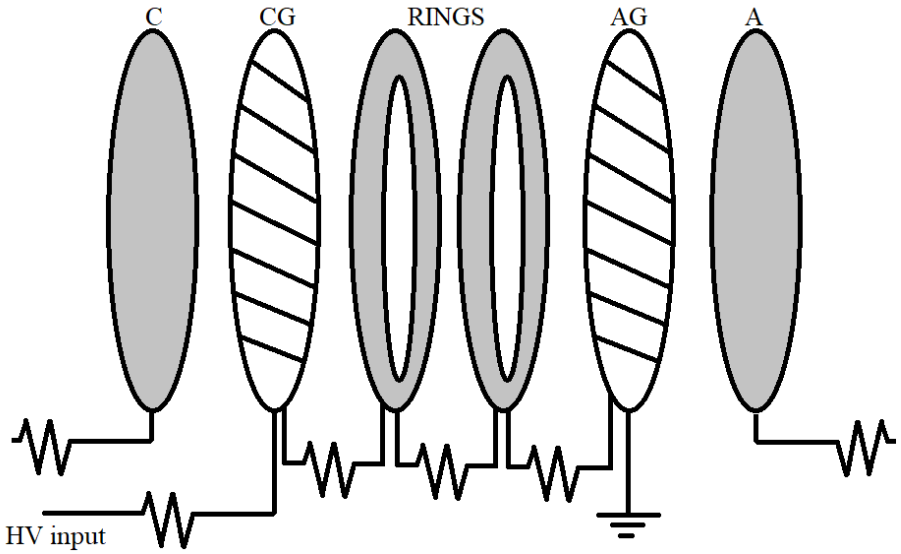

Figure 2.1: Scheme of the experimental apparatus. From the left, there is the cathode (C), the cathode grid (CG), two rings, the anode grid (AG) and the anode (A). The cathode grid, the two rings and the anode grid are connected through three resistances; the cathode, the cathode grid and the anode can be provided high voltage through three voltage supplies (one each). The drift path between the cathode and the anode is 5.1 cm.

locally, reaching high values and helping the onset of electron amplification.

The anode, the cathode and the cathode grid are connected to a high voltage power supply each, in order to be able to change the three voltages independently; the anode grid, instead, is always grounded. To set the voltages, one must take into account that, in order to make the electrons see the grids as transparent, not all values of electric potential difference between anode and anode grid, and cathode and cathode grid, work: for example, a good ratio between V_C and V_{CG} is $V_C/V_{CG} \sim 1.5$. Besides, since the current crosses a resistance R=125 MΩ between the high voltage power supply and the components, and since the cathode grid is part of the bigger circuit that involves the 3 resistances of 50 MΩ, the rings and the grounded anode grid, the effective voltage at the cathode grid, V_{CG}, is different from the voltage that is set, V_{in}, the relation being:

$$V_{CG} = V_{in} \frac{3 \cdot 50}{125 + 3 \cdot 50} \tag{2.1}$$

The amount of charge that moves through the areas between the cathode and the cathode grid, and the anode grid and the anode gives two signals that pass through a pre-amplifier and are finally read by the software LabView. The signal that is collected is a couple of waveforms (one for the signal at the

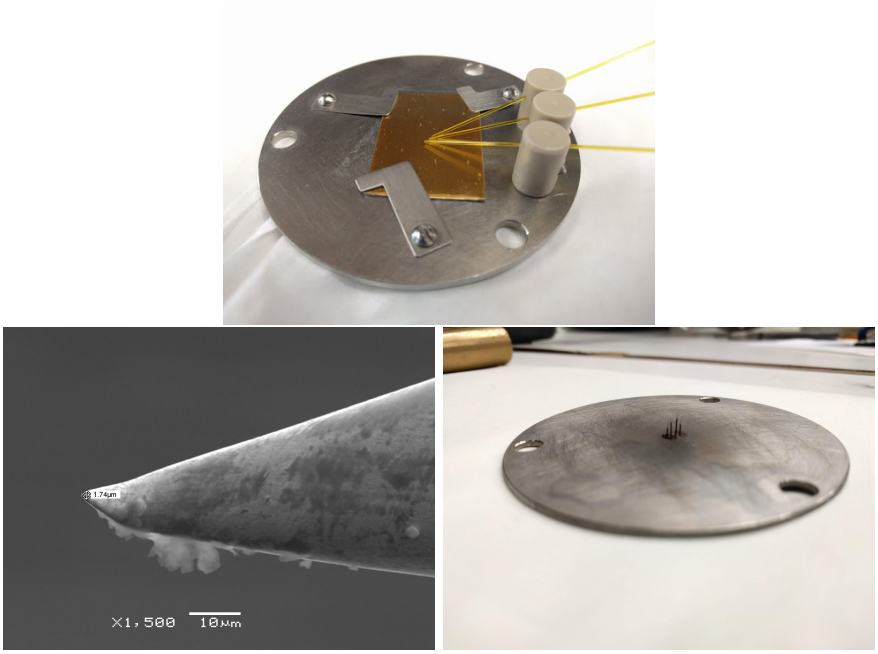

Figure 2.2: Top: cathode used for LArCADe and some optical fibers that are used to extract the electrons. Bottom: a tip as seen with an electron microscope (left) and the tips soldered to the anode (right).

anode and one for signal at the cathode) which show the trend of the charge (corresponding to the amplitude of the waveforms) as a function of time. The anode signal results in a positive waveform, since the charge is approaching the anode, while the cathode signal gives a negative waveform, since the charge is leaving the cathode. For each measurement, 50 consecutive couples of waveforms are automatically recorded.
One important fact to notice is that the pre-amplifier distorts the two signals, the distortion being greater when the drift time of the electrons is greater, and depending on the RC constant of the pre-amplifier; the pre-amplifier that was used is characterized by a RC constant $\tau_{RC} = 240$ μs. To take into account this distortion, a RC correction had to be calculated.

2.2 Run 1

Run 1 was performed in April 2018, and measures in Liquid Argon were taken: the apparatus, without tips on the anode, was put into a dewar and immersed in LAr; measurements were then taken, setting the cathode voltage and the cathode grid, respectively, to V_C = -200 V and V_{CG} = -130 V (the value that was actually set for the cathode grid is V_{in} = -230 V); the anode grid was grounded, while the voltage for the anode was changed in a range ∼13 - 1000 V. This run was able to provide some data to compare to data

in Run 2, in which tips were present, in order to establish the effect of the tips themselves.
The measurements that were taken during this run are of two kinds:

A) Data taken at the same voltages, during a 10-hour-long interval of time; with increasing time, the fraction of electrons that reach the anode could vary if the purity of Argon changes.

B) Data taken at fixed values of V_C and V_{CG}, but varying V_A. The typical trend of signals for this kind of data taking is the following: with increasing voltages, the fraction of electrons that reach the anode becomes greater and greater since the transparency of grids also increases; at a certain point, the amount of electrons reaching the anode becomes stable with increasing voltages; at high enough voltages, if there is the onset of amplification regime, the fraction of electrons reaching the anode increases again.

Data were preliminarily analyzed by Fava & Caratelli through the following procedure:

- Firstly, noise was removed, by performing a Fourier transformation and deleting signals with high frequencies ($>$ 20 Hz); in Figure 2.3, on the left, an example of the Fourier transform of a signal before and after noise removal is shown: the black line shows that background is partly made of high frequencies that do not appear in the signal; on the right of Figure 2.3 there is the superposition of a waveform before and after noise filtering. Although some noise remains, the waveform was considered good enough to perform further data analysis; moreover, it was observed that removing frequencies lower than 20 Hz would have biased the amplitude of the signals.

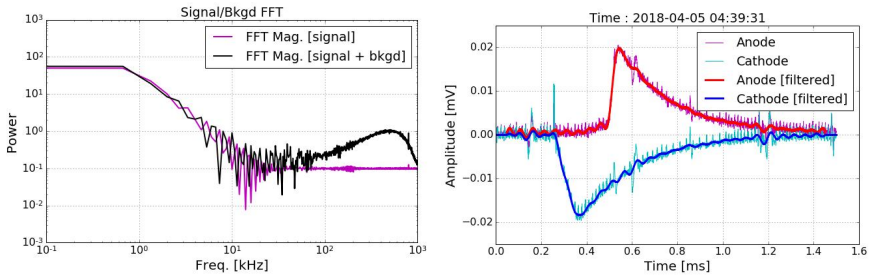

Figure 2.3: On the left: comparison between frequencies of signal + background (black curve) and of signal only (magenta curve); on the right: comparison between waveforms before and after noise filtering. Graphs by D. Caratelli & A. Fava.

- After noise filtering, two quantities were considered: the maximum/minimum for the anode/cathode waveform, and the drift times from the anode

grid to the anode, and from the cathode to the cathode grid; this quantity was calculated by looking for the times at half height and at maximum/minimum, and by multiplying by two the difference:

$$t_{drift} = \frac{t(max) - t(h/2)}{2} \tag{2.2}$$

- For the data of type A, the trend of signals' maximum/minimum and of drift time as a function of time were studied. The results can be seen in Figure 2.4.

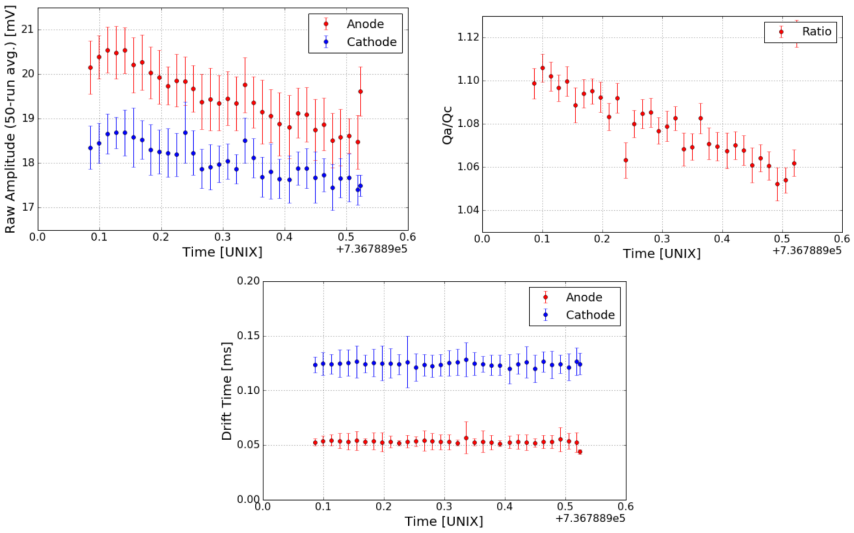

Figure 2.4: Above: absolute value of maximum/minimum for the anode/cathode signal (left) and ratio between the two quantities (right). Below: drift time of electrons in the area between the cathode and the cathode grid (blue dots) and between the anode grid and the anode (red dots). All the quantities are as a function of the time, referring to a 10-hour-long data taking. Plots by D. Caratelli & A. Fava.

- For the data of type B, instead, the trend of signals' maximum/minimum and of drift velocity as a function of anode voltage were considered. The results can be seen in Figure 2.5.

During the internship time, the data analysis procedure was refined, and the data of type B were re-analyzed through the new method. The improved procedure is as follows:

- the noise was filtered in the same way, removing frequencies > 20 Hz;

- to estimate the RC correction, the drift time t_{drift} is computed doubling the time between the point at which the waveform is at 1/4 of its height, and the point at which it is at 3/4 of its height; the drift

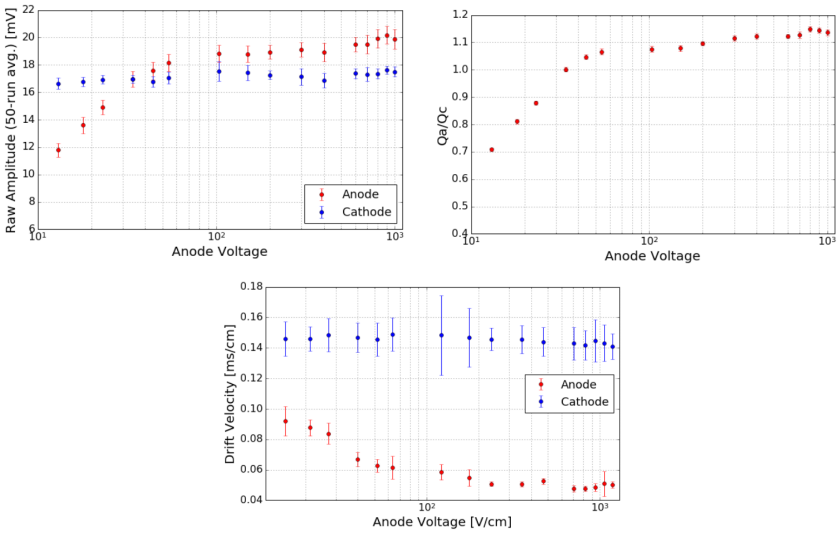

Figure 2.5: Above: absolute value of maximum/minimum for the anode/cathode signal (left) and ratio between the two quantities (right). Below: drift velocity of electrons in the area between the cathode and the cathode grid (blue dots) and between the anode grid and the anode (red dots). All the quantities are as a function of the anode voltage. Plots by D. Caratelli & A. Fava.

time is then used to compute the correction factor

$$CF_{RC} = (1 - e^{-t_{drift}/\tau_{RC}}) \cdot \frac{\tau_{RC}}{t_{drift}} \tag{2.3}$$

The values of maximum/minimum found in the waveforms have to be divided by CF_{RC} in order to obtain the correct value. Moreover, the waveforms' baselines are shifted with respect to zero: to have the right value for the amplitudes, the value of the baseline has to be subtracted from the maximum/minimum, before proceeding with the RC correction and further calculations;

- the value of the maximum/minimum of the waveforms, corrected for the baseline, is found for each of the 50 measurements at the same anode voltage; this will be useful to estimate the error for the maximum/minimum, as the RMS divided by the square root of 50;

- the mean waveform is computed, averaging the 50 measurements, and the value of the maximum/minimum of the signals is found, corrected for the baseline and the RC constant.

- finally, the relative difference between the maximum of the anode signal and the absolute value of the minimum of the cathode signal is found:

$$\Delta Q = \frac{\max(A) - |\min(C)|}{|\min(C)|} \tag{2.4}$$

The results of the new analysis of Run 1 data are reported in Figure 2.6: comparing them to the preliminary data analysis, one can see that the raw amplitudes shown in Figure 2.5 correspond to the uncorrected amplitudes in Figure 2.6; the RC correction has little effect on the anode signal for which, in fact, the drift time is shorter, while it affects significantly the cathode signal, which becomes greater than the anode signal, as expected. The new procedure to obtain the drift times, instead, yields smaller values: the reason for which it was introduced, indeed, was that the values obtained with the old procedure seemed to be biased towards larger values since, obviously, the waveforms decrease significantly their sloping near the maximum/minimum: choosing not to consider this area to compute the drift time seemed to provide more accurate estimations.

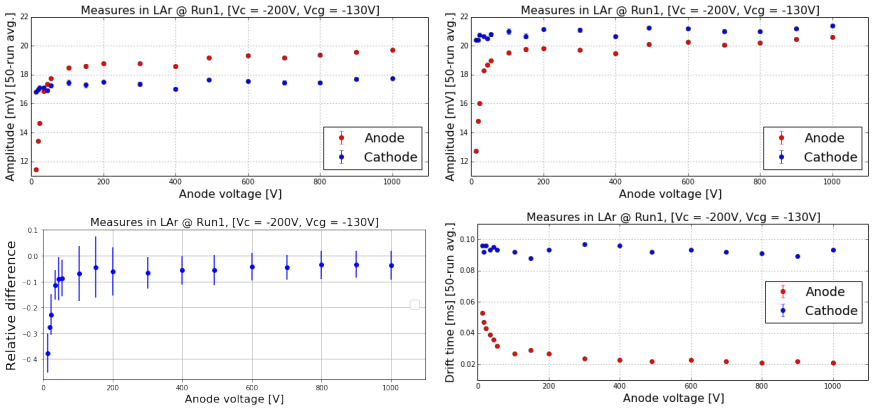

Figure 2.6: Above: absolute value of maximum/minimum for the anode/cathode signal without RC correction (left) and with RC correction (right). Below: one the left, relative difference ΔQ between the anode and the cathode signal for Run 1 data taking; on the right, drift times of electrons in the area between the cathode and the cathode grid (blue dots) and between the anode grid and the anode (red dots). All the quantities are as a function of the anode voltage.

2.3 Run 2

Run 2 was performed in August, and for this run the four tips were added. First of all, the response of the pre-amplifier was checked, by using a wave generator. In Figure 2.7 the results are reported: the response of the pre-amplifier is linear, as wished.

After that, vacuum was made inside the dewar "Blanche", located at the laboratory "PAB" at Fermilab, which contained the experimental apparatus for this run. When the pump had lowered the pressure to $P \sim 7 \cdot 10^{-3}$ Torr, to remove H_2O residuals, some baking was also performed: modifying the voltages in one designated module, some resistances were correspondingly

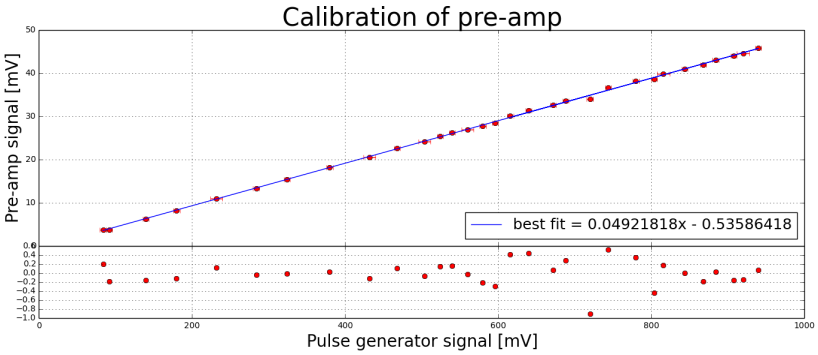

Figure 2.7: Response of the pre-amplifier to waves of different amplitude.

changed, and the temperature inside Blanche also varied. The pressure increased again as the H_2O detached from the walls, to $P \sim 2$ Torr, then decreased again as the H_2O was aspirated by the pump. When a pressure $P \sim 2.5 \cdot 10^{-5}$ Torr was reached the data taking was started. The vacuum configuration was used to check the behavior of the nine fibers connected to the photocathode: the fibers were inserted into the UV lamp one at once, and the signals at the cathode and at the anode were recorded. The voltages were set at the following values:

* V_C = - 50 V
* V_{CG} = - 30 V
* V_A = 25 V

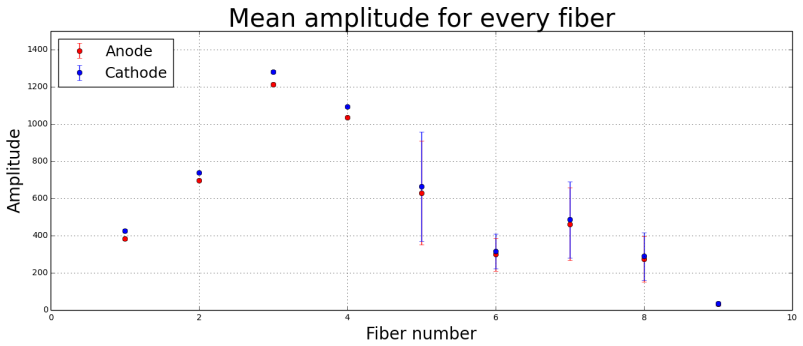

Figure 2.8: Amplitude of signals at the cathode (blue dots) and at the anode (red dots) relative to the nine optical fibers used in the experiment. For the fibers 1, 2, 3, 4 only one measurement was taken, for the remaining 5 fibers the points are the mean of 10 different measurements, and the error bars the RMS.

For every fiber (except fibers number 1, 2, 3, and 4) 10 measurements were taken, each time removing and inserting again the fiber into the lamp, in

order to reduce the dependence to the incidence angle between the light and the fiber; for the remaining 4 fibers, only one measurement was taken. The results can be seen in Figure 2.8: there are systematic fluctuations in fibers response, both from one measurement to another with the same fiber, and from one fiber to another; since in vacuum there is no amplification, and the signal recorded is relative to the whole anode (plate and tips) these can only be intrinsic variations, not due to position with respect to the tips.

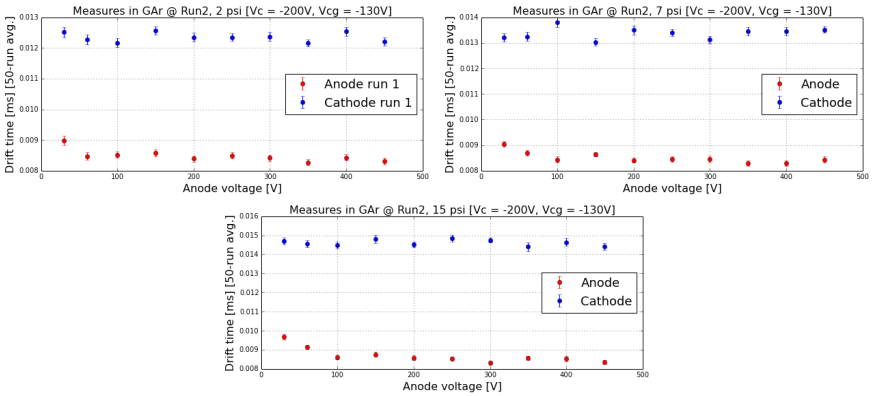

Figure 2.9: Drift times in gas at 2 psi (top left), 7 psi (top right), and 15 psi (bottom).

For measures in gas, data were taken at three different values of pressure: 2, 7 and 15 psi; the voltages that were set are the following:

* V_C = - 200 V
* V_{CG} = - 130 V

while the anode voltages were changed in a range 30 - 450 V for each value of pressure. The fibers used for this phase were all but 1 and 6.

The data were analyzed through the improved procedure described in Section 2.2; in the case of gaseous Argon, however, also the 50 waveforms were RC-corrected. The results of the analysis are reported in Figures 2.9 (drift times), 2.10 (amplitudes) and 2.11 (relative amplitudes): from Figure 2.11 the three phases of increasing transparency, steadiness, and amplification are easily visible; in gas, however, the amplification was already expected.

Finally, liquid Argon was put into Blanche and data were taken with the same configuration as with gaseous Argon (the same values for V_C and V_{CG} and the same fibers); this time, anyway, a broader range for anode voltages was probed (46-1000 V). The results of data taking in liquid Argon can be seen in Figure 2.12: from the comparison of drift times between data of Run 1 and Run 2 (top graph) it is easy to see that the drift times in this run are

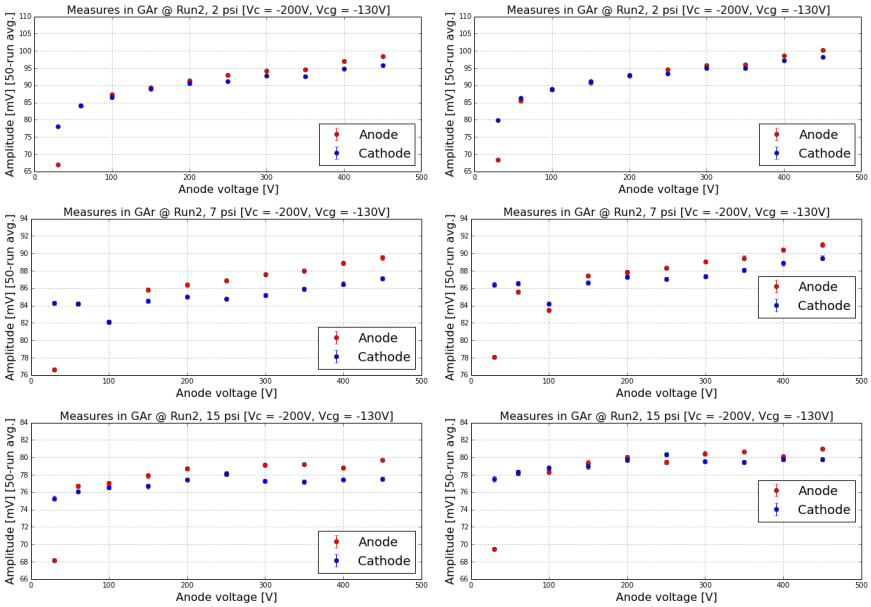

Figure 2.10: Amplitude of signals in gas at 2 psi (top figure), 7 psi (center), and 15 psi (bottom); on the left, the values are raw (the RC correction was not applied); on the right, the plots are shown after applying the RC correction.

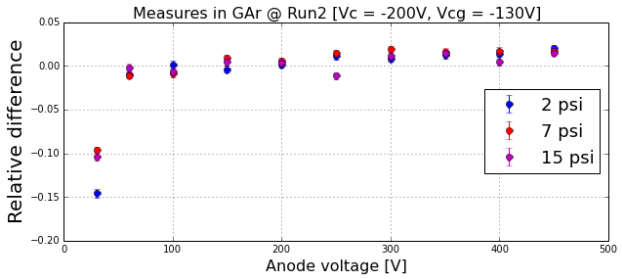

Figure 2.11: Relative amplitude at 2 psi (blue dots), 7 psi (red dots), and 15 psi (violet dots).

systematically higher than times in the previous run, perhaps due to a lower purity of the liquid Argon that was used. Moreover, from the bottom graphs emerges that no amplification seems to be produced.

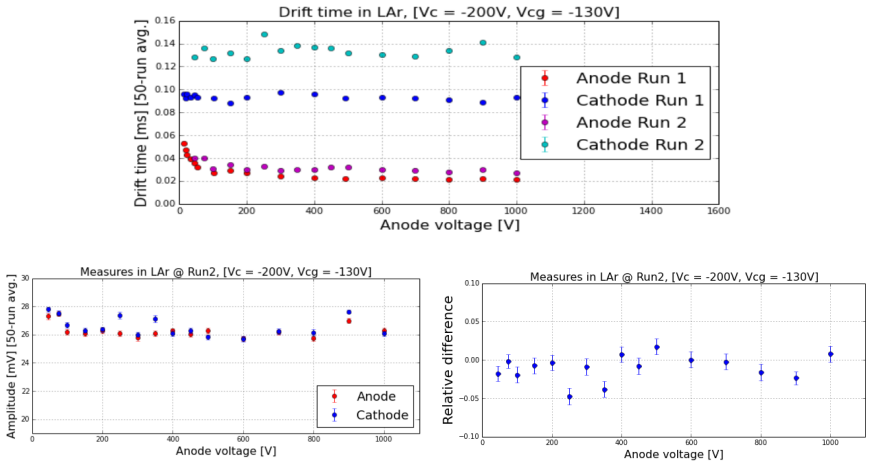

Figure 2.12: Drift times in LAr measured in Run 2 compared to data collected in Run 1 (top), amplitudes at the anode and at the cathode (bottom left), and relative difference between the two signals (bottom right), as a function of anode voltage.

A fit of the rising part of the signal was also tried, and residuals were calculated, in order to see whether there were any small peaks which could point out some amplification. An example is shown in Figure 2.13; neither this study has provided any evidence for the onset of amplification.

2.3.1 Multiplication factor in LAr

Using data taken in LAr, an attempt to estimate the multiplication factor was carried out in the following way:

- Since the drift time was known thanks to the analysis described above, and the distance between the anode and the anode grid was measured before Run 1, the drift velocity v_{drift} was determined;

- The electric field E can be found inverting the formula

$$v_{drift} = \mu E \tag{2.5}$$

with

$$\mu = \frac{a_0 + a_1 E + a_2 E^{3/2} + a_3 E^{5/2}}{1 + (a_1/a_0)E + a_4 E^2 + a_5 E^3} \left(\frac{T}{T_0}\right)^{-3/2} \tag{2.6}$$

where a_0=551.6, a_1=7953.7, a_2=4440.43, a_3=4.29, a_4=43.63, a_5=0.2053, and T_0=89 K are constants defined on lar.bnl.gov/properties/trans.html.

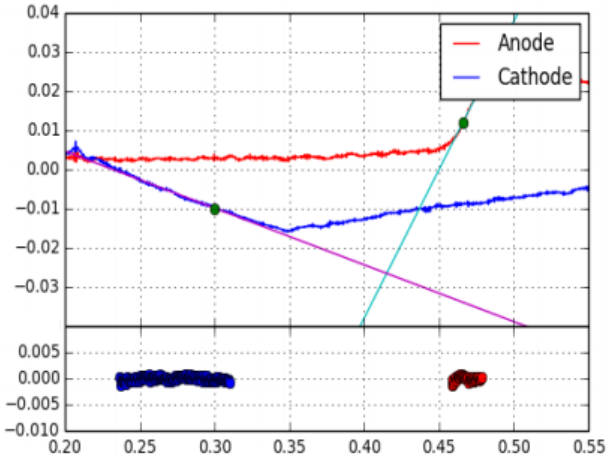

Figure 2.13: Example of linear fit of a signal collected in liquid Argon (above), with $V_A = 250$ V, and relative residuals (below); all fits and residuals with different values of V_A do not show deviations from linearity, which could be a sign of small amplifications. Thr anode and cathode waveforms are zoomed to better show the linear fit.

- Since the mean ionization potential for Argon is 23.6 eV, and the mean free path in LAr is 0.65 nm, to have electrons which are energetic enough, an electric field $E \geq 3.6 \cdot 10^8$ V/cm is needed.

- In areas where the electric field is high enough, each time an electron ionizes an Argon atom, a new free electron is provided; a first approximation of the multiplication factor M can be, hence:

$$M = 2^{L/d} \tag{2.7}$$

  where L is the distance between the anode and the anode grid, and d is the mean free path. This is only a rough approximation, however, since it does not take into account factors such as the cross section between electrons and Argon atoms.

Calculating the electric field with this method provided too low values for the electric field, yielding no amplification; however, the values found are relative to the average electric field in the area between the anode and the anode grid, while it is possible that the electric field reaches high enough values only very close to the tips.

2.4 Simulations with COMSOL

In order to better understand what to expect from the experiment, some simulations were performed, with focus for the phase with gaseous Argon; the simulations were implemented with the 5.3a version of the software "COMSOL Multiphysics".

COMSOL Multiphysics is a "a general-purpose simulation software" that helps to "understand, predict, and optimize physics-based designs and processes with numerical simulation" (https://www.comsol.com/products).

2.4.1 Setup of the simulation

The purpose of the simulation was to reproduce a simplified version of the experiment, composed of two plates (representing the anode grid and the anode) and one single tip on the anode; after that, an electric potential had to be applied and the trajectories of some electrons had to be computed. To achieve this goal, first of all it was necessary to become familiar with the software, and this was attained with the help of COMSOL guide (COMSOL, 2011) and of the work of Ziac (2012). After that, the simulation was built according to the following steps, described in detail to make it possible to recreate the simulation:

- **GEOMETRY**:
  The first step in the simulation was to define all the setup's parts, as listed in Table 2.1; apart from the experimental apparatus, an additional cone was build in between the tip and the cathode, in order to exploit the disk-shaped base as starting point for the particles. The result was the setup shown in Figure 2.14.

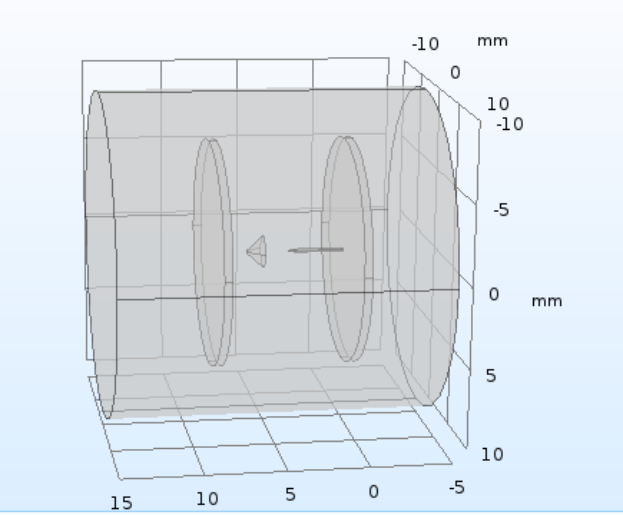

Figure 2.14: Simulated experimental apparatus after building all geometry elements.

- **MATERIALS**:
  the materials that were used are copper for the cathode plate and the whole anode, while the dewar was filled with argon (inlet cone included). Copper was a built-in material, while gaseous argon was

Element	Shape	Parameters	Location
Cathode	Cylinder	Radius: 7 Height: 0.5	x: 0 y: 0 z: 7.9
Anode plate	Cylinder	Radius: 7 Height: 0.5	x: 0 y: 0 z: -0.5
Tip support	Cylinder	Radius: 0.1 Height: 3	x: 0 y: 0 z: 0
Tip	Cone	Bottom Radius: 0.1 Height: 0.5 Top Radius: 0.001	x: 0 y: 0 z: 3
Tip end	Sphere	Radius: 0.001	x:0 y: 0 z: 3.5
Dewar	Cylinder	Radius: 10 Height: 20	x: 0 y: 0 z: -5
Particle inlet	Cone	Bottom Radius: 1 Height: does not matter Top Radius: does not matter	x: 0 y: 0 z: 5

Table 2.1: Geometry elements, listed in the same order as they were defined in the simulation. On the top of the tip a little sphere was built, in order to smooth the tip end; the anode parts (plate, tip support, tip and tip end) were joined through a union, keeping input objects and interior boundaries; this union was then joined with the cathode plate with the same options. After the dewar was built, the difference was created between the dewar itself and the latter union; at the end "Form Union" was build. All the quantities in the Table are expressed in mm.

simulated starting with built-in air; the only parameter requested to compute the electric field, and that had to be set in this phase, was the relative permittivity; it was put equal to 1 to simulate the gaseous argon.

- **PHYSICS**:
The simulation consisted of two phases, the computation of the electric field in the entire experimental setup, and the study of particle trajectories in that electric field. Therefore, two physics modules were used, correspondingly the Electrostatics and the Charged Particle Tracing ones.
In the *Electrostatics* module, in "Ground" the cathode was selected as the domain; an "Electric Potential" was added, and here the domain was made of the whole anode. In the "Electric Potential" window the potential to apply to the anode can be set.
In the *Charged Particle Tracing* module, the "Massless" formulation was chosen; in fact, this allows to accurately model the drift velocity of the electrons, which is the dominant factor to affect the particles' motion (Ziac, 2012). For this reason, in "Particle Properties" electrons' velocity was set as follows:

$$\begin{aligned} v_x &= -4000. * es.E_x/sqrt(es.E_x^2 + es.E_y^2 + es.E_z^2) \\ v_y &= -4000. * es.E_y/sqrt(es.E_x^2 + es.E_y^2 + es.E_z^2) \\ v_z &= -4000. * es.E_z/sqrt(es.E_x^2 + es.E_y^2 + es.E_z^2) \end{aligned} \tag{2.8}$$

measured in m/s. The factor 4000 represents the mobility of electrons in argon.
For the wall properties, the anode and the cathode were selected as domain, and the "Stick" condition was set, in order to make the particles stop if they reached one of the electrodes; finally, in the "Inlet" window the disk-shaped base of the inlet cone was chosen as domain, and the number of particles per release was set as equal to 1000.

- **MESH**:
in order to run a simulation with COMSOL, the geometry objects must be meshed: this means that a sort of grid is created all over the elements, defining the intersection points where COMSOL performs the calculations; the mesh can be of different shapes and more or less refined. To obtain precise values, especially near the tip, an "extremely fine" mesh was chosen, made of free tetrahedrons. The result is shown in Figure 2.15.

- **STUDIES**:
the last step before launching the simulation was to set the parameters of two studies, correspondent to the two different physical modules:

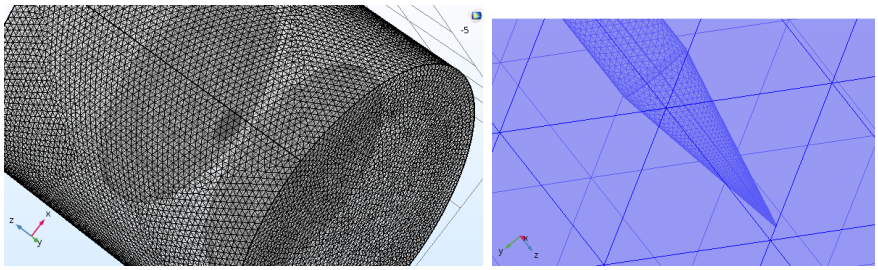

Figure 2.15: Left: mesh obtained for the whole setup. Right: mesh detail near the tip.

the former, relative to the computation of the electric field in the experimental setup region, was a *stationary* study, while the latter, to study the particle trajectories, was *time dependent*; the trajectories were simulated for a time interval $\Delta t = 5 \cdot 10^{-6}$ s, discretized into 10000 parts. In Figure 2.16 an example of the outcome of the two studies can be seen.

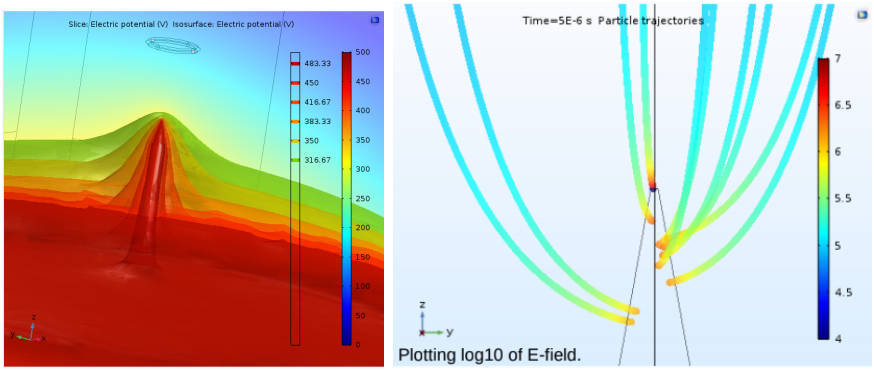

Figure 2.16: Left: electric potential in the area near the tip. Right: trajectory of electrons ending onto the tip (outcome of a simulation with only 10 particles); the colors of the trajectory indicate the strength of the electric field.

The simulation allowed to collect data about the position of the particles and the electric field felt by them in their path between the disk and the tip, at different values of the electric potential, that was varied in a range 0-900 V; the data were then analyzed in order to calculate the multiplication factor of the electrons. However, it is immediately clear from the right picture in Figure 2.16 that the electric field, at least in the simulation, becomes strong only in the immediate vicinity of the tip.

2.4.2 Analysis of the simulated data

The data collected were analyzed following the procedure described by Sauli (1977): in gaseous Argon, the inverse of the mean free path for a particle,

α, called *Townsend coefficient*, can be approximated as

$$\alpha = P \cdot A \cdot e^{B \cdot P/E} \tag{2.9}$$

where P is the gas pressure, E is the electric field, and A and B are equal to, respectively, 14 cm^{-1} $Torr^{-1}$ and 180 V cm^{-1} $Torr^{-1}$. This approximation is valid for low values of α, and was considered good for LArCADe setup with GAr. α can then be used to obtain the multiplication factor of electrons M though the formula

$$M = \exp\left(\int_{x_1}^{x_2} \alpha(x)\, dx\right) \tag{2.10}$$

For the data collected in the simulation, the integral was turned into a sum. For every simulated particle M was computed for three different values of pressure (2, 7 and 15 psi); M as a function of the particle's initial distance from the tip on the x-y plane was then plotted for every value of P and of the electric potential (see Figure 2.17, top left, for an example). The 1000 values of M for every value of P and of the electric potential were then averaged. The result is reported in Figure 2.17 (bottom); from this plot what emerges is that the average multiplication factor per particle is higher when gas pressure is lower. To compare the result with the expected analytical trend, D. Caratelli plotted it for the three values of pressure considered in the analysis (Figure 2.17, top right): it is clear from this plot that, for low enough values of the electric field, the multiplication factor is indeed higher for lower pressure; a possible interpretation can be that, at lower pressure, the larger mean free path lets electron reach high enough energy to ionize atoms even at low electric fields; when the electric field increases, instead, and the electrons easily reach the threshold energy for ionization, the larger number of atoms at higher pressures is the prevailing factor.The trend obtained with the simulation data appears, anyway, consistent with the expected multiplication factors, since the particles travel for the most part of their trajectories in low enough electric fields.

2.5 Run 3

To have further data to compare with the simulations, a new run in gaseous Argon was performed, changing a bit the experimental setup: for instance, the anode grid and the cathode grid were rotated by 60 degrees, since it was suspected that the wires were covering the tips in the previous run, and the resistances were soldered again to the rings; moreover, the device was inserted into a smaller dewar than Blanche; finally, this time all the 9 fibers were used.
Three different pressures were probed: 3, 7 and 15 psi, reaching voltages higher than in Run 2 with GAr (this time V=1000 V was reached). When

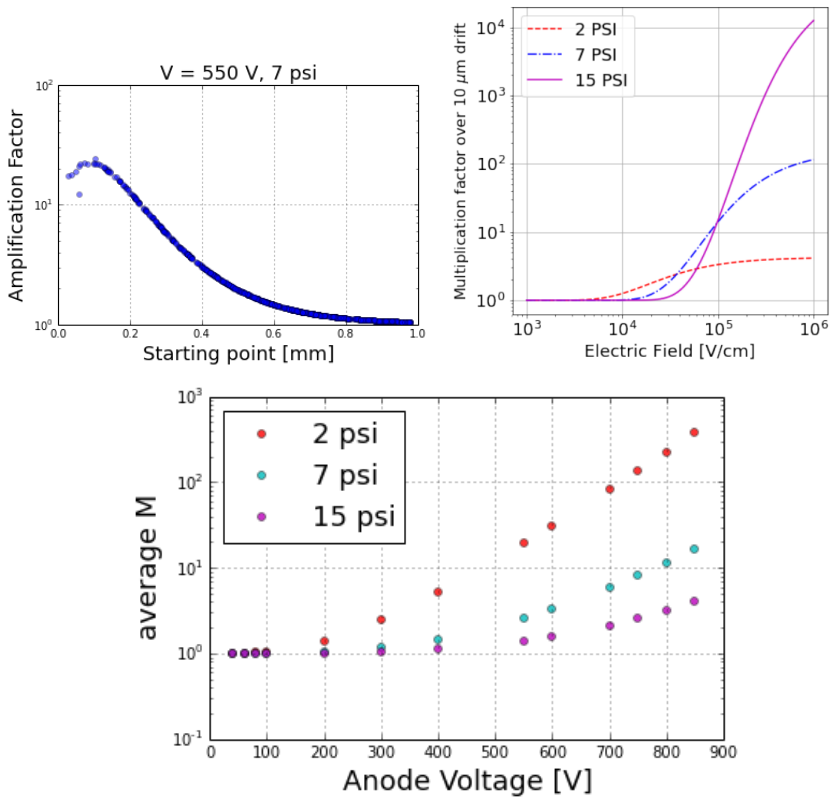

Figure 2.17: Top left: example of multiplication factor M as a function of the particle's initial distance from the tip on the x-y plane; the anode voltage that was set in the simulation in this case is 550 V, and the data were analyzed for a pressure $P = 7$ psi. Top right: plot by D. Caratelli, showing the expected trend of M as a function of the electric field; at low enough electric fields, M is higher for lower pressures. Bottom: average M as a function of the anode voltage, for pressures $P = 2$, 7, and 15 psi; M turns out to be higher for lower pressures, consistently with the analytical trend.

high voltages were reached, however, the waveforms broadened for some reason that still has to be figured out (see Figure 2.18, left): for this reason, the data analysis had to be modified to take this effect into account. It was decided to consider the areas under the waveforms instead of looking for the peaks; for this analysis, then, no RC correction was calculated. The results of the analysis are shown in Figure 2.18, right: in the graph, the relative difference of the anode and the cathode signals is plotted as a function of the anode voltage. The three phases of increasing transparency of the grids, of stabilization, and of amplification can be distinguished clearly; furthermore, the amplification is higher for lower pressure, consistently with the simulation results described in Section 2.4.2.

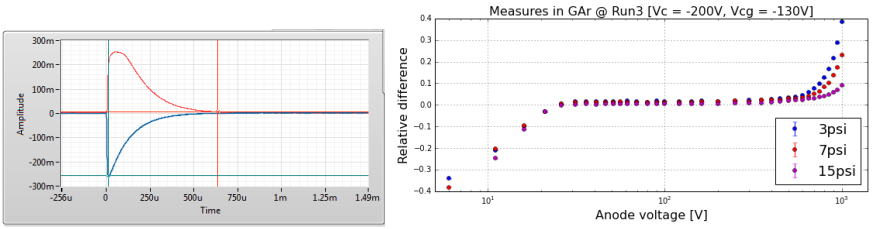

Figure 2.18: Left: waveforms relative to the anode and cathode signals at $V_A = 1000$ V. The waveform relative to the anode (red curve) is broadened for still unknown reasons. Right: relative difference between the anode and the cathode signal as a function of anode voltage for data taken at P = 3 psi (blue dots), 7 psi (red dots), and 15 psi (violet dots).

2.6 Setup of Raspberry Pi camera

When data are taken in liquid Argon, a possible effect the strong electric field near the tips could bring is to heat the LAr so much, that some bubbles form; this would be an undesirable phenomenon, since it would bring instability to the multiplication of electrons. To check whether some bubbles really form or not, it was decided to monitor the tips with a Raspberry Pi camera (Figure 2.19, top), inside a glass dome pipe, put into the dewar; since the glass dome pipe still had to be tested when the internship ended, it was not possible to perform a new run in LAr with the camera during that period, nevertheless the camera was prepared and some tests were conducted outside the dewar to check the performance of the camera.
First of all, the camera was connected to the board, and then configured it following the instructions on the website
https://projects.raspberrypi.org/en/projects/getting-started-with-picamera;
the code controlling the camera enables it to take both pictures and videos. The focus of the camera was then adjusted in order to take unblurred pictures at a distance (27 ± 4) cm, which will be the distance between the camera and the tips in Blanche. To check this, pictures were taken every

centimeter moving the camera with the laboratory's light on; one example can be seen in Figure 2.19, bottom left. To take pictures inside Blanche, nevertheless, a source of light will be needed to see the tips: to provide it, four white LEDs were also connected to the board, fixed around the camera and set up with the help of the website https://learn.pi-supply.com/bright-pi-v1-0-code-examples/, turning their gain and their brightness up. The experimental setup and the camera were then covered with black canvases, and pictures were taken again: the result is similar to the one obtained with the laboratory's light on (Figure 2.19, bottom right); although the tips are quite small, they are visible, and it is very likely that also bubbles will be revealed, if they form.

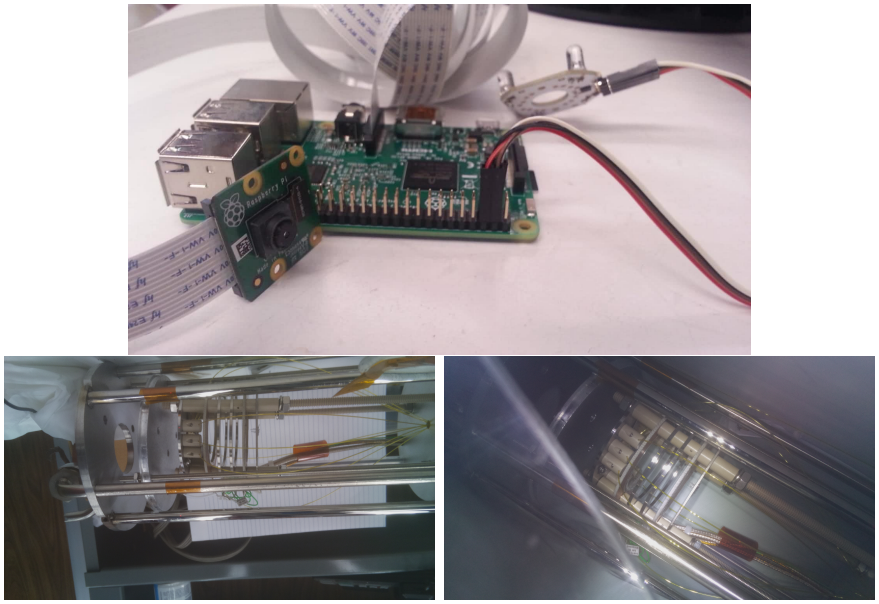

Figure 2.19: Top: picture of the Raspberry Pi camera (front), the board (center) and the LEDs (background). Bottom left: picture taken with the Raspberry Pi camera with the laboratory's light on; bottom right: picture taken with the Raspberry Pi camera with the experimental setup covered and the small LEDs on.

Chapter 3

Conclusions

During the internship period, two runs with tips were performed: run 2, using gaseous Argon and then liquid Argon, and run 3, only with gaseous Argon. Moreover, the data analysis method was refined, and also data taken previously with liquid Argon and without tips, in Run 1, were re-analyzed. From data taken in GAr, both in Run 2 and in Run 3, amplification at high voltages is evident, as expected; this results will be a useful calibration for further measurements. In liquid Argon, however, no amplification was observed, neither in Run 1, as predicted, nor in Run 2, which theoretically could have been possible instead. This could be due to improvements that are needed in the experimental setup: for example, the effect of the tips could be enhanced now that the grids have been rotated by 60 degrees. Apart from this, future plans include the preparation of new tips, with a smaller radius ($\sim$ 100 nm), which will enable to reach higher electric fields, and help the onset of electron amplification. Another problem that could affect the experiment is the possible formation of bubbles in heated LAr near the tips, because of the strong electric field; to investigate whether or not they form, a Raspberry Pi camera was prepared to monitor the tips, and a new run with LAr is planned, as soon as the glass dome pipe to contain the camera is tested.
One further question that arose during the work is what fraction of electrons actually reaches the tips, since the anode signal included both electrons that reached the anode plate and electrons collected by the tips. Hence, it would be useful to perform a new run covering the anode plate, in order to see only the electrons that end up onto the tips.
The simulation that was performed was useful to better understand the experiment, however it was run only for GAr, and involved a simplified version of the apparatus; some improvements that could be made are to simulate also LAr, and make the experimental setup more similar to the real one. Simulating the setup with liquid Argon would also solve the problems explained in Section 2.3.1 to calculate the multiplication factor in LAr, since

the discretization of the electrons' path would allow to consider only regions close to the tips, which at least in the simulation are the only ones with high enough electric fields.

Bibliography

[1] Althüser, L., 2015, "GEANT4 simulations of the Münster dual-phase TPC", bachelor thesis

[2] Aprile, E., Contreras, H., Goetzke, L. W., Melgarejo Fernandez, A.J., Messina, M., Naganoma, J., Plante, G., Rizzo, A., Shagin, P., & Wall, R., 2014, "Measurements of proportional scintillation and electron multiplication in liquid xenon using thin wires", JINST 9 P11012

[3] ARIS Collaboration, 2018, "Measurement of the liquid argon energy response to nuclear and electronic recoils", Phys. Rev. D 97, 112005

[4] BNL website lar.bnl.gov/properties/trans.html

[5] Chepel, V., & Araújo, H., 2013, arXiv:1207.2292v3

[6] COMSOL Multiphysics, 2011, "Introduction to COMSOL Multiphysics"

[7] COMSOL website, https://www.comsol.com/products

[8] DEAP-3600 Collaboration, 2018,"First results from the DEAP-3600 dark matter search with argon at SNOLAB", Phys. Rev. Lett. 121, 071801

[9] Kim, J. G., Dardin, S. M., Jackson, K. H., Kadel, R. W., Kadyk, J. A., Peskov, V., & Wenzel, W. A., 2002, "Studies of electron avalanche behavior in liquid argon", IEEE Trans. Nuc. Sci. 49 1851-1856

[10] MicroBooNE Collaboration, 2012, MicroBooNE Technical Design Report, lss.fnal.gov/archive/design/fermilab-design-2012-04.pdf

[11] Murphy, S., 2016, arXiv:1611.05846

[12] Policarpo, A. P. L., Chepel, V., Lopes, M. I., Peskov, V., Geltenbort, P., Ferreira Marques, R., Araújo, H., Fraga, F., Alves, M. A., Fonte, P., Lima, E. P., Fraga, M. M., Salete Leite, M., Silander, K., Onofre, A., & Pinhão, J. M., 1995, "Observation of electron multiplication in liquid xenon with a microstrip plate", Nucl. Instr. Meth., vol. A365, pp. 568-571

[13] Raspberry Pi camera tutorial, https://projects.raspberrypi.org/en/projects/getting-started-with-picamera

[14] Raspberry Pi LED tutorial, https://learn.pi-supply.com/bright-pi-v1-0-code-examples/

[15] Sauli, F., 1977, "Principles of operation of multiwire proportional and drift chambers", CERN 77 - 09

[16] Ziac, J., 2012, "Numerical Simulation of the Electric Field and the Study of the Electron Collection Efficiency in a Xe TPC"